

# Visualization of Multiscale Ring Formation in a Rotary Kiln

Lee Rippon<sup>1</sup>, Barry Hirtz<sup>2</sup>, Carl Sheehan<sup>3</sup>, Travis Reinheimer<sup>4</sup>, Philip Loewen<sup>1</sup>, and  
Bhushan Gopaluni<sup>1</sup>

<sup>1</sup>*University of British Columbia, Vancouver, B.C., Canada*

<sup>2</sup>*Cool Cameras, Prince George, B.C., Canada*

<sup>3</sup>*Spartan Controls, Burnaby, B.C., Canada*

<sup>4</sup>*Canfor Pulp, Vancouver, B.C., Canada*

## Abstract

Rotary kilns are large-scale unit operations that are critical to many industrial processes such as cement production, pyrometallurgy, and kraft pulping. As expensive, energy-intensive units, it is imperative from both an economic and environmental perspective to ensure efficient operation of the rotary kiln. To provide additional insights for operation and maintenance, rotary kilns are increasingly outfitted with more advanced sensing technology. Leveraging this supplementary data requires strategies and active efforts towards storage, processing, and visualization. In this work we provide a visualization strategy for industrial thermal camera data that is measured along the shell profile of a rotary lime kiln. The proposed strategy assists specifically with the visualization of ring formation at different timescales, but it also serves more generally as a useful tool for operations management. This paper describes the visualization strategy, provides a demonstration with industrial data, and offers open-source resources for interested users to implement it themselves.

**Keywords**— data visualization, lime kiln, process monitoring, recausticizing, ring formation

## 1 Introduction

Rotary kilns are enormous cylindrical vessels that serve as key unit operations in cement production, pyrometallurgy and kraft pulping. Industrial rotary kilns consist of a slightly inclined steel shell, lined with refractory bricks, rotated by a drive gear, and supported on tyres and rollers. Since these are very expensive vessels that operate at high temperatures (often exceeding 1000°C), preventative maintenance is important for rotary kiln management and safety. Moreover, the high energy intensity of rotary kilns and their fundamental role in many industrial processes provides a strong motivation to keep them operating as efficiently as possible (Gürtürk and Oztop, 2014).

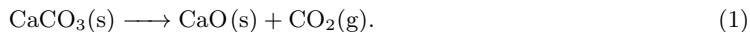
To address maintenance and operations challenges, rotary kilns are increasingly outfitted with more sophisticated technology for kiln monitoring and control. One such example is the use of infrared thermal cameras to measure the shell temperature along the length of the kiln. In addition to identifying hot-spots and preventing damage to the kiln refractory, these thermal cameras can provide insight into aspects of the kiln operation such as fouling or ring formation (Danila and Tamas, 2020). As more kilns are equipped with thermal cameras, it becomes increasingly important to extract value from this data. Representing the data in a visually intuitive manner is critical for extracting and communicating process insights from large quantities of operating data.

The contributions of this paper include introducing a novel, user-friendly approach to visualizing large quantities of kiln shell temperature (KST) profiles at varying timescales. Our proposed approach was developed specifically to visualize the formation of rings in a rotary lime kiln which may grow and decay on a timescale between days and months. An industrial case study from a lime kiln in a kraft pulp mill is presented to demonstrate the effectiveness of the proposed approach for visualizing the formation of rings and investigating additional disruptions to kiln operation. The software used to develop the shell profile visualization is entirely open-source and the license permits commercial applications. A tutorial for running the visualization with synthetic kiln data is provided (Rippon, 2020) along with implementation

resources as a further contribution to the community of rotary kiln professionals who may wish to implement this visualization strategy on their own data. Ultimately, the objective of this work is to help improve the production efficiency of kiln operations by providing enhanced data visualization techniques and resources that empower operators and engineers to gain improved insights from historical operating data.

## 2 Background

Although the proposed visualization technique applies generally to rotary kilns, here we elaborate on our study of a lime kiln in the kraft pulping process to provide more background and insight. Lime kilns are used in kraft pulping to regenerate calcium oxide (i.e., lime) from calcium carbonate (i.e., lime mud) according to the following endothermic calcination reaction (Tran, 2007):



Lime mud is fed to the top of the inclined rotary kiln where it begins to dry into a powder before agglomerating into nodules in the preheating zone. The preheating zone facilitates an increase in temperature of the kiln solids from approximately  $80^\circ\text{C}$  to about  $870^\circ\text{C}$  at which point the calcination reaction begins (Gorog and Leary, 2016). Approximately 3 MJ of energy is required to produce 1 kg of pure CaO at  $900^\circ\text{C}$ . Rotary lime kilns can be over 4 m in inner diameter while exceeding 100 m in length (Dernegård et al., 2017). The lime moves through the kiln in about 2 to 3 hours depending on the speed of rotation (typically around 1 rpm) and the slope of the kiln (approximately  $2^\circ$ ) (Smook et al., 1982).

The most troublesome problem for lime kiln operation is the formation of rings (Tran, 2007). These are annular cylinders formed by adhesion and accumulation of lime mud or product lime particles to the refractory wall on the inside of the kiln, which restrict the flow of gas and solids in the kiln. Ring orifices can reduce lime production; purchasing lime instead of producing it on site can cost over \$50,000 per day. Moreover, if the ring goes unnoticed it can result in overheating and damage to the kiln’s refractory lining, which may require repairs and lost production in excess of \$3 million per event (Gorog and Leary, 2016). Rings can form at significantly different rates, with noticeable deposits accumulating quickly over a matter of days, or gradually over a matter of months. This large variation in the timescale of formation creates challenges for detecting and visualizing ring growth.

Recently, thermal imaging tools (e.g., infrared cameras) have become significantly more affordable while offering better performance and functionality. This has led to increased interest in these cameras for modeling and monitoring of rotary kilns (Le Guen and Huchet, 2020)(Yi et al., 2013). Thermal imaging cameras can be installed along the length of the kiln shell, as shown in Figure 1, to monitor the shell temperature profile for abnormal situations. One common abnormal situation is the occurrence of shell hot spots, which are indications of potentially dangerous refractory failure. Another important application for thermal cameras is the detection of ring formation in a lime kiln (Hirtz et al., 2017).

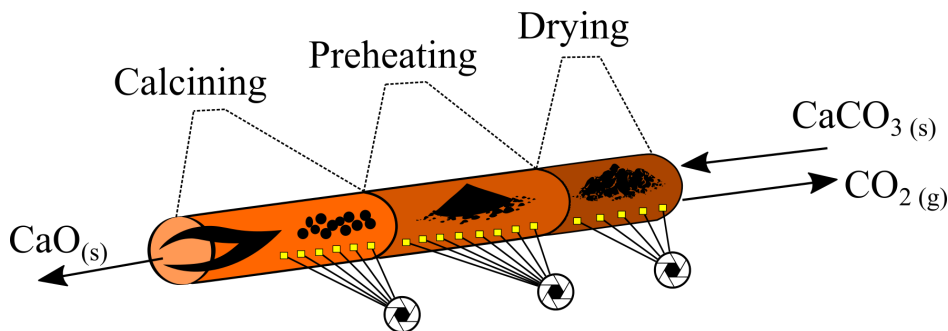


**Figure 1:** A simplified illustration of rotary lime kiln with three thermal cameras. Lime mud is fed into the kiln where it is dried into a powder and then agglomerated into nodules which are calcined into lime product.

As thermal camera technology is increasingly deployed to kilns an abundance of historical KST data

is generated and the potential for data-driven optimization of kiln operating policies becomes increasingly realizable. Extracting robust insights from this deluge of historical data requires active efforts towards data storage, processing, and visualization. A variety of devices can be used to collect KST measurements including handheld pyrometers, one-dimensional line scanners that use a rotating head, and two-dimensional thermal cameras with a fixed field of view such as those illustrated in Figure 1. Moreover, the data acquired from these various devices can be used in several ways to visualize the KST profile and the formation of rings. The synthetic data in Figure 2 illustrates a simple example of a common KST visualization technique whereby a handheld pyrometer is used to manually collect KST measurements at different locations along the kiln. Infrequent manual measurements are combined and

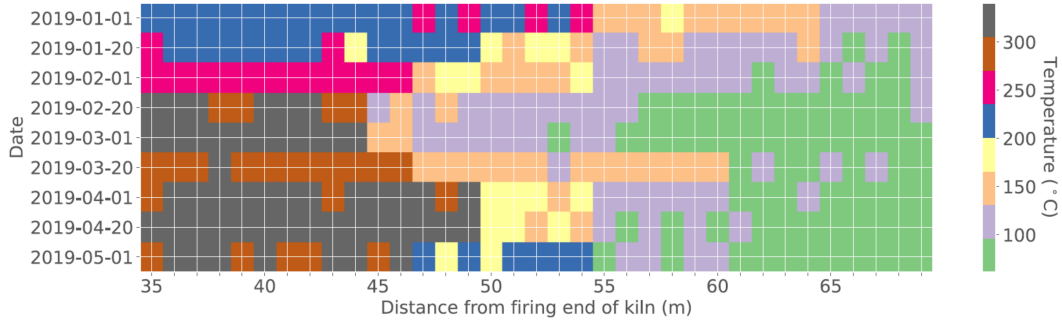


**Figure 2:** Synthetic data illustrating a low-resolution map of KST profiles. These maps are typically constructed from infrequent manual measurements whereby someone is tasked with measuring the KST at different positions by walking along the kiln with a handheld pyrometer (Keim et al., 2020).

used to construct a low-resolution map of KST profiles over time with a qualitative color map (Keim et al., 2020). The proposed approach improves this situation by enhancing the resolution, intuitiveness, and interactivity of the visualization while also collecting and processing the data using existing thermal cameras instead of manual pyrometer readings.

The continuous two-dimensional thermal camera data can be averaged over a day and stitched together to generate a KST profile as shown in Figure 3. The synthetic data shown in Figure 3 illustrates a

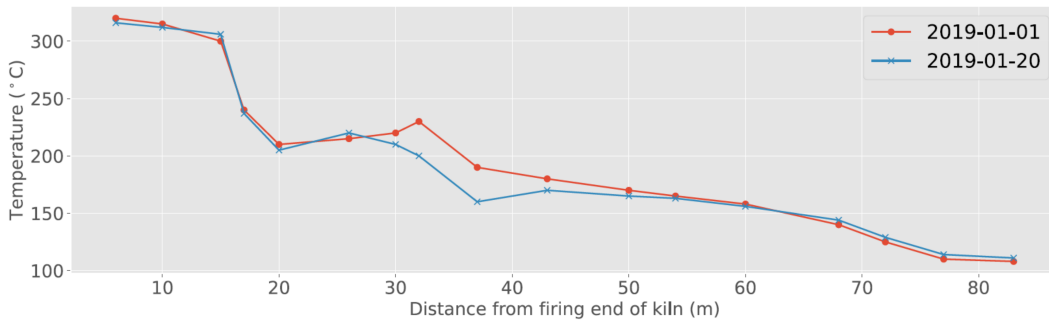


**Figure 3:** Synthetic thermal camera measurements are averaged over a day and stitched together to generate a KST profile. The synthetic KST profile from 2019-01-01 represents measurements taken after the kiln was cleaned and the profile from 2019-01-20 is overlaid to emphasize changes to the profile and potential ring formation.

straightforward approach to visualizing ring formation. Data from 2019-01-01 represents measurements taken from a clean KST profile after a maintenance shutdown. It is compared to measurements after twenty days of operation to visualize potential ring growth between 30-45 m from the firing end of the kiln. Alternatively, a line scanner can be calibrated with the rotation speed of the kiln to visualize the entire outer shell of the kiln over a single rotation period, as illustrated by Figure 4. The visualization technique illustrated by the synthetic data in Figure 4 provides insights along the tangential dimension (or outer circumference) of the kiln shell along the  $y$ -axis in addition to the axial KST variations along

the  $x$ -axis.

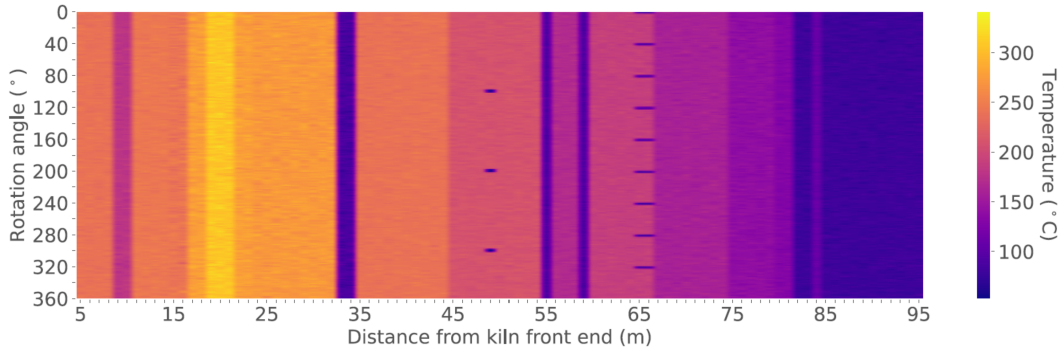


**Figure 4:** A synthetic illustration of a kiln shell scan measured over a single rotation period. These visualizations are often produced by one-dimensional line scanners that use a rotating head calibrated to the rotation speed of the kiln.

One drawback of the visualization illustrated by Figure 4 is the lack of a temporal dimension to provide insights into the evolution of the KST profile over time (e.g., during ring formation). Besides, as the kiln rotates approximately once per minute it may become infeasible (or at least undesirable) to process and store high dimensional images for each rotation. A strategy analogous to that shown in Figure 3 is possible whereby an earlier clean shell profile is compared to a shell scan from a later date to investigate changes. However, in practice this amounts to a cumbersome side-by-side comparison of separate shell scan images that can overwhelm practitioners when large quantities of historical data need to be analyzed. The proposed visualization strategy overcomes limitations of these existing methods by providing an intuitive visualization of large quantities of data that clearly illustrates the evolution of KSTs across any user-specified timescale. Moreover, the proposed technique is complementary to visualizations with two spatial dimensions (e.g., Figure 4 or raw camera images). The proposed multiscale visualization can be used to identify periods of interest from which to investigate further with raw images.

A straightforward, user-friendly, and open-source method for visualizing the formation of rings in a rotary kiln over varying timescales with KST profiles from thermal infrared cameras is described in the following section.

### 3 Methodology

The methodology presented here addresses two important aspects of visualizing the formation of rings in a rotary kiln. Firstly, the conversion of raw KST data from a thermal camera to a visually intuitive spatiotemporal heatmap is presented. This is followed by the development of a user-friendly interactive approach to controlling the timescale at which kiln temperature dynamics are observable.

#### 3.1 A heatmap of the shell temperature profile

Consider a matrix of KST measurements,  $\mathbf{T}(\mathbf{x}, \mathbf{t})$ , where the rows of  $\mathbf{T}$  are indexed by  $\mathbf{x} = [x_1, x_2, \dots, x_n]$  and the columns of  $\mathbf{T}$  are indexed by  $\mathbf{t} = [t_1, t_2, \dots, t_\tau]$ . Each  $x_i$  represents the distance from the firing end of the kiln that the thermal camera measurement is taken whereas each  $t_i$  represents a periodic sequence of discrete sampling times with a total of  $\tau$  samples. Each row,  $i$ , of  $\mathbf{T}$  is a univariate time series,  $T(x_i, \mathbf{t})$ , composed of  $\tau$  total KST measurements at position  $x_i$  from the firing end of the kiln. Each column,  $j$ , of  $\mathbf{T}$  is a snapshot of the entire KST profile at time  $t_j$ , denoted  $T(\mathbf{x}, t_j)$ .

The KST measurement positions,  $\mathbf{x}$ , are determined by the placement and commissioning of the thermal camera(s) along the kiln which may result in positions that are not equispaced. If these non-equispaced positions are not properly addressed they can create obscurities while visualizing large numbers of KST profiles which can in turn cause misleading conclusions about the spatial dynamics in the kiln. A snapshot of a non-equispaced KST profile at time  $t_j$  is presented in Figure 5. Each temperature

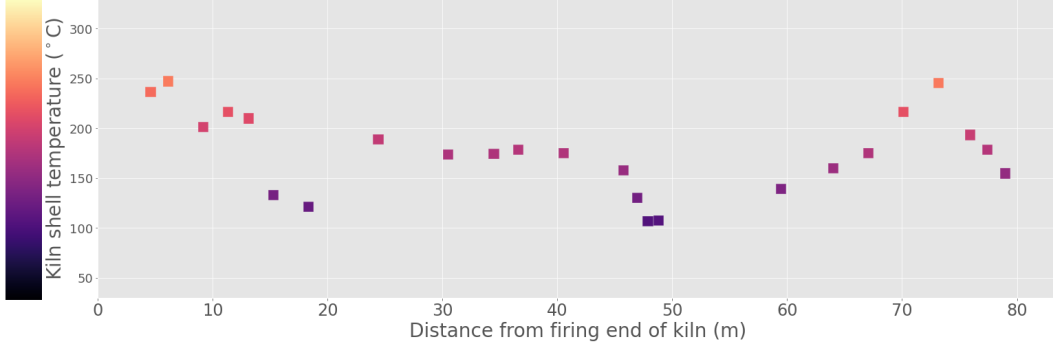


**Figure 5:** A sample of the KST profile with non-equispaced measurement positions. Two-dimensional thermal cameras use discrete measurement areas to summarize thermal camera pixels into a single temperature measurement at fixed positions and intervals.

in Figure 5 is assigned a distinct color, as shown in the color bar on the left. Each observation is plotted in its assigned color, effectively embedding the  $y$ -axis as uniform, sequential colors, as a precursor to further refinements below.

To address the non-equispaced samples we create an upsampled KST profile,  $\tilde{T}(\mathbf{x}, \mathbf{t})$ , by performing piecewise linear interpolation on positions between those provided in the original row index, i.e.,  $x_i < x < x_{i+1}$ . Since the interpolation is only along the spatial dimension, we can drop  $\mathbf{t}$  for notational simplicity. The simplest piecewise linear interpolation function defined on  $[x_1, x_n]$  that reproduces the measured temperatures is

$$\tilde{T}(x) = T(x_i) + \frac{x - x_i}{x_{i+1} - x_i} [T(x_{i+1}) - T(x_i)] \quad \text{for } x_i < x < x_{i+1}. \quad (2)$$

Repeating this interpolation for all positions defined on  $[x_1, x_n]$  yields the up sampled KST profile which is presented for the same sample time in Figure 6. Once again, the  $y$ -axis values map directly to the

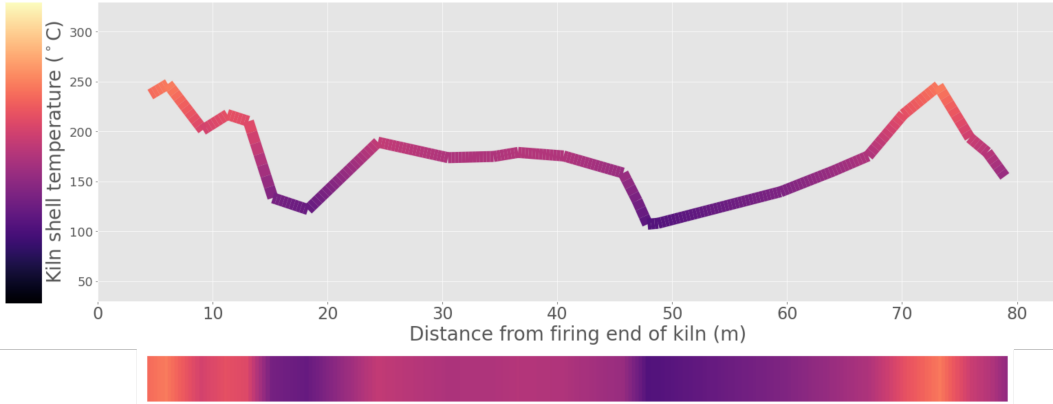


**Figure 6:** Piecewise linear interpolation of the KST profile. The bottom color bar embeds the  $y$ -axis temperatures with a uniform, sequential colormap enabling a clear and intuitive single-axis visualization for engineers and operators.

vertical color bar legend on the left-hand side. The horizontal image at the bottom of Figure 6 represents the same KST profile but with the  $y$ -axis embedded in the colors according to the legend. Rotating this image clockwise by  $90^\circ$  provides one column from our up sampled KST matrix  $\tilde{T}(\mathbf{x}, \mathbf{t})$ . Repeating this process for all samples yields an image of  $\tilde{T}(\mathbf{x}, \mathbf{t})$  that enables a visually intuitive representation of large quantities of KST data.

There are many options for selecting the colormap used to represent kiln temperatures, but to be

consistent, it is recommended to select one that resembles the raw thermal camera images. Once measurements with invalid magnitudes are addressed, the maximum and minimum values of  $\tilde{\mathbf{T}}$  are mapped to opposite ends of the colormap. Intermediate values are mapped in a uniform fashion with equal increases in temperature yielding equal increases along the colormap. The resulting visualization is a spatiotemporal heatmap of the rotary kiln over  $\tau$  sampling periods.

### 3.2 Visualization at multiple timescales

If the scale,  $\tau$ , over which we visualize the KST data is too large then high frequency ring formation dynamics occurring on a time scale of, for example, days instead of years, will be compressed into a small number of pixels rendering them incomprehensible. To visualize the KST profile at varying time scales parameters for the start date ( $s$ ) and the window size ( $w$ ) are specified by users. The window size defines the number of samples that the user would like to visualize while the start date determines where to place the window in the historical database. As demonstrated in the tutorial, an interactive user-interface is programmed into the visualization to provide convenient specification of the start date and window size (Rippon, 2020). Ultimately, we are left with an up sampled slice of the raw KST matrix, i.e.,  $\tilde{\mathbf{T}}(\mathbf{x}, t_{s:s+w})$ , which we use to analyze the KST profile of the kiln. In the following section we introduce a case study of an industrial rotary lime kiln, and we demonstrate the use of this heatmap to visualize the formation of rings at multiple timescales.

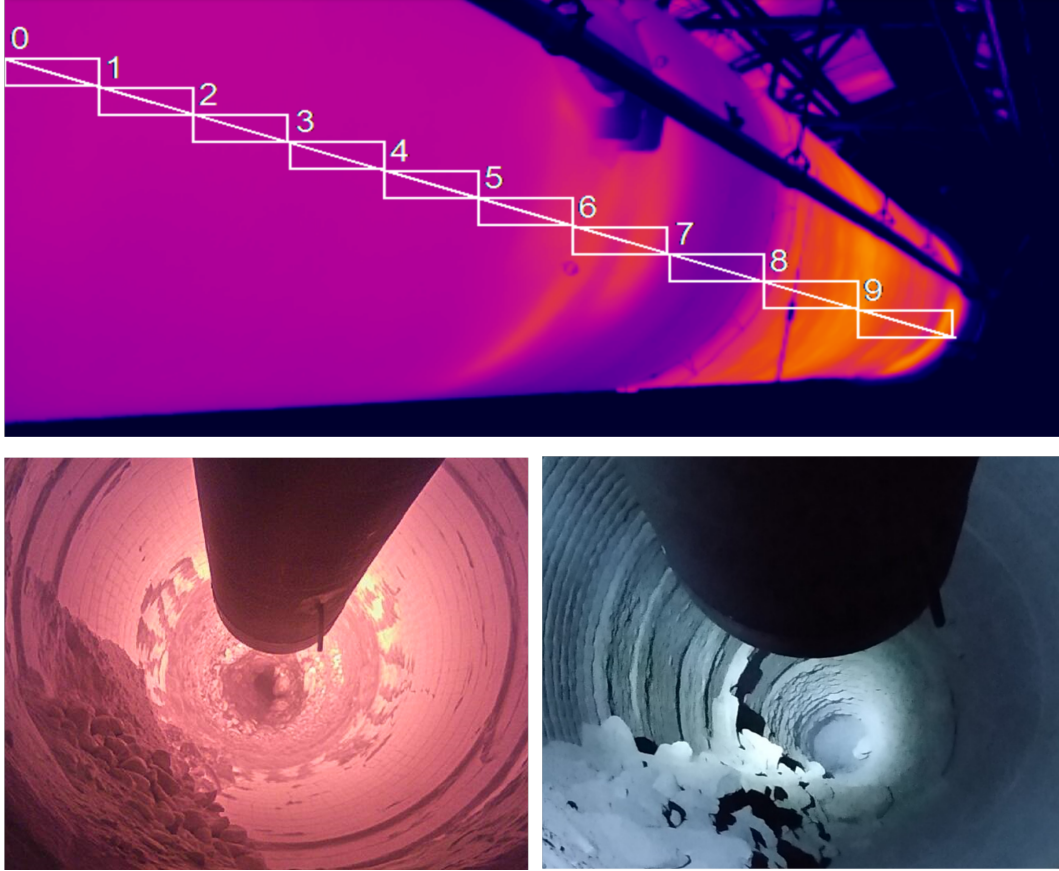
## 4 Industrial Case Study

Consider an industrial rotary lime kiln in a kraft pulping process that is approximately 85 m long and 3 m in diameter. The kiln is the most energy intensive unit operation in the process and plays an essential role in driving  $\text{CO}_2$  off of  $\text{CaCO}_3$  to restore the causticity of  $\text{CaO}$  so that it can be used to recausticize green liquor. Like many kilns, this kiln is challenged by the formation of rings such as those shown in Figure 7. For improved control and management of abnormal situations (such as rings) this kiln has been equipped with a large amount of instrumentation, including thermal infrared cameras.

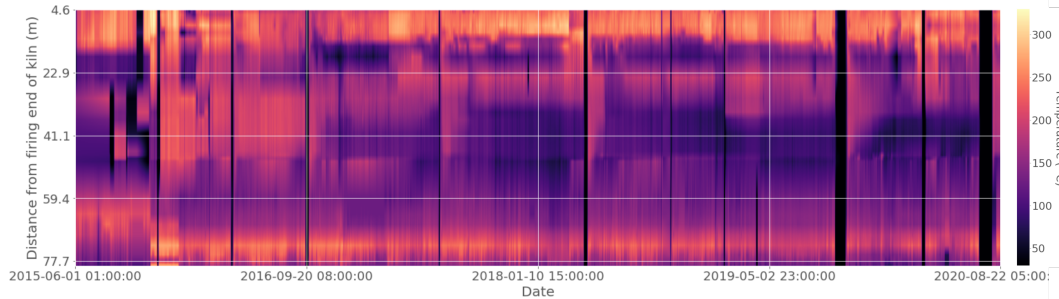
The imaging resolution for each thermal camera is  $480 \times 360$  (width  $\times$  height) temperature measurements taken 30 times per second. To satisfy historian storage constraints the axial width of each data bin is set to approximately 3 meters (although this can be adjusted to be larger or smaller) and the data is reported to the historian every minute. The thermal cameras are capable of measuring temperatures between  $-40^\circ\text{C}$  to  $1500^\circ\text{C}$  with an accuracy of  $\pm 2^\circ\text{C}$ . Although we have access to more frequent samples, hourly averages provide a sufficiently high temporal resolution for visualizing the formation of rings at multiple time scales over a five-year history (over 45,000 samples).

The rotary lime kiln under study is equipped with three thermal cameras that measure the shell temperature profile at non-equispaced locations along the kiln. Although each camera logs ten measurements in the historian, two measurements from each camera are omitted in the proposed visualization because they are related to the external bracing around the kiln. A total of 24 KST measurements are sampled along the length of the kiln creating a shell temperature profile with measurements spanning between 4 to 79 meters away from the firing end of the kiln. To analyze the formation of rings at varying time scales a database of KST profiles and other relevant process variables (PVs) is extracted using hourly averages from more than five years of historical operation. The matrix of raw KST profiles ( $\mathbf{T}$ ) are up sampled as previously described and the resulting matrix ( $\tilde{\mathbf{T}}$ ) is used to generate the spatiotemporal heatmap in Figure 8.

The  $y$ -axis of the heatmap shows the distance from the firing end of the kiln in meters while the  $x$ -axis provides the date of the KST profile. An accompanying legend, mapping the heatmap colors to shell temperatures in degrees Celsius is included on the right side of Figure 8. An intuitive correlation of the shell temperature with the brightness of the heatmap color provides immediate operating insights, e.g., the vertical black slices are from prolonged maintenance shutdowns. Just to the right of 2018-01-10 (in the middle of Figure 8) we see a shutdown followed by a period of presumed fouling at approximately 20-40 m from the firing end of the kiln. The fouling is presumed because the KST profile becomes significantly darker (indicating lower temperature) along that section of the kiln while remaining relatively stable at both the firing end and feed end of the kiln. By conveniently specifying the start date and window size we can quickly visualize a slice of  $\tilde{\mathbf{T}}$  to better investigate this period of presumed fouling, as shown by



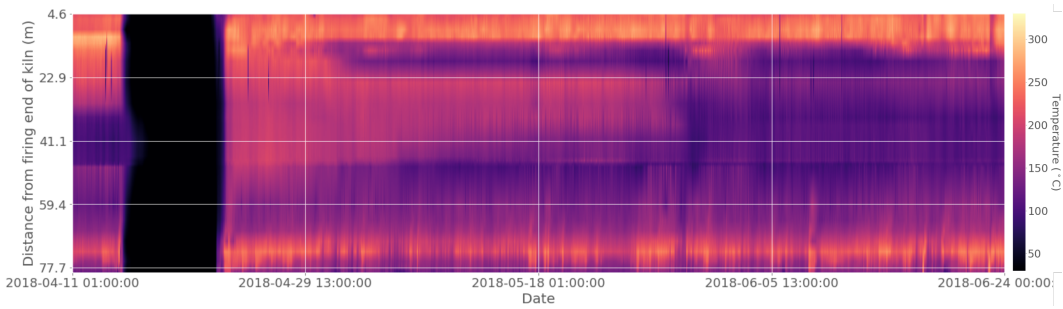
**Figure 7:** **Top:** kiln shell image from thermal camera with ten rectangular temperature measurement areas. **Bottom left:** burning zone ring. **Bottom right:** stress fracturing of ring into debris with thermal cycling.



**Figure 8:** Spatiotemporal heatmap of KST profiles spanning over 5 years of operation. To our knowledge this is the only proposed visualization of KST data that provides a clear and intuitive view of the shell temperature profile evolution over years of operation. Note that no special processing of KST measurements was performed to account for internal kiln components such as chains or internal lifters.

the heatmap of  $\tilde{T}(\tilde{x}, t_{s:s+w})$  in Figure 9.

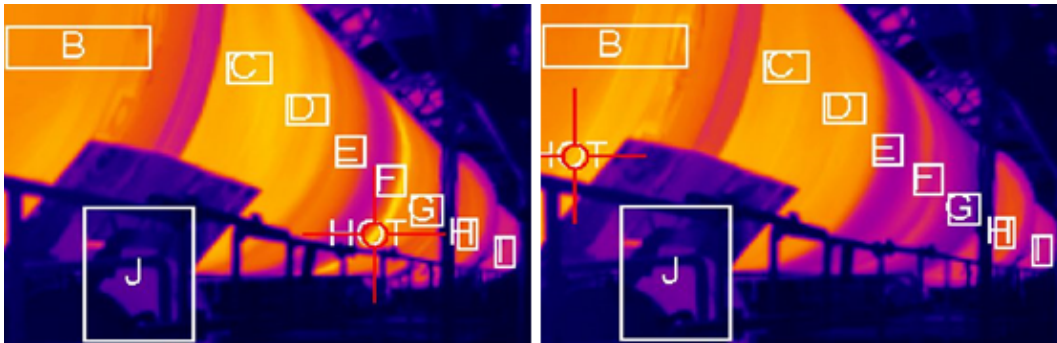
By reducing the window size and studying Figure 9 we can obtain some more insights into this period of ring growth. One thing to note from Figure 9 is that a ring appears to form after 2018-04-29 at approximately 18 m from the firing end of the kiln. Another observation from Figure 9 is that a much longer ring appears to form between approximately 23-40 m from the firing end of the kiln. The



**Figure 9:** Focusing on a period of presumed fouling. Note, potential ring formation is observed after 2018-04-29 at approximately the 18 m and 45 m positions, respectively. Afterwards, between 2018-05-18 and 2018-06-05 the presumed ring appears to begin to bridge these separate formations and extend into the 23-40 m range.

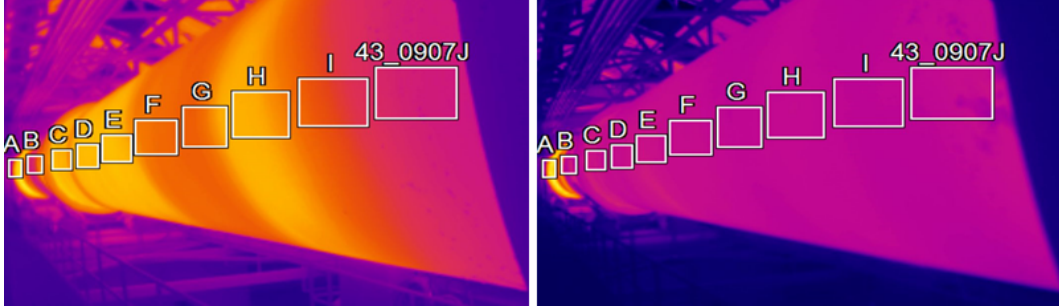
presumed formation of this longer mid-kiln ring happens between 2018-05-18 and 2018-06-05. Given these more specific periods of interest we can either narrow the periods down further by reducing the window size of our visualization tool or if we have sufficient specificity, we can move on to inspecting the raw thermal camera images from these time periods directly. In this case we have selected the latter choice to demonstrate how the proposed visualization strategy complements the raw thermal camera images.

Figure 10 compares two raw thermal images taken from the camera on the firing end of the kiln. The



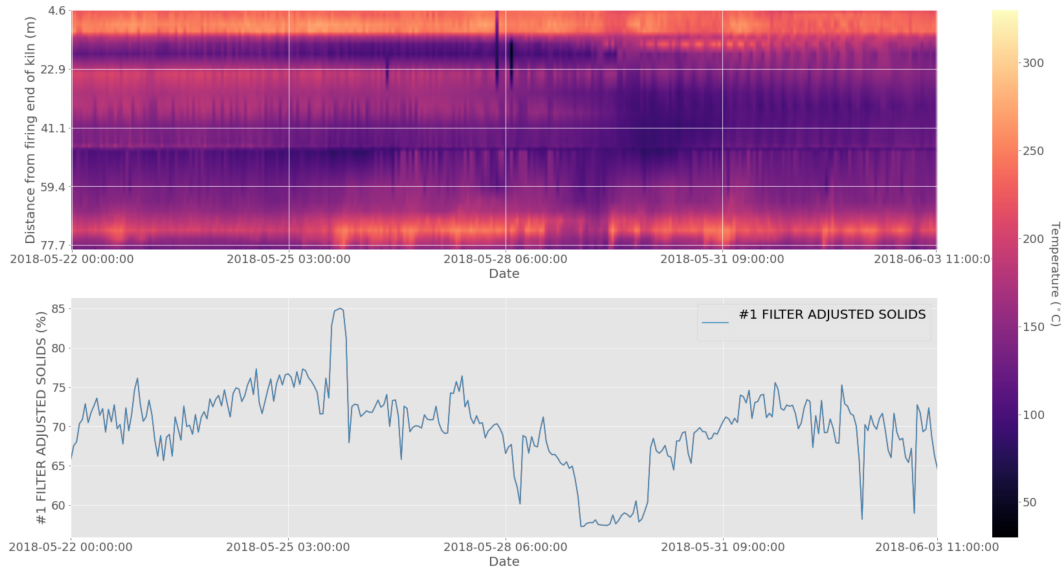
**Figure 10:** Investigating raw thermal camera images to confirm the presumed ring formation approximately 18 m from the firing end of the kiln just after 2018-04-29. **Left:** an image from the firing end camera taken on 2018-04-29. **Right:** another image from the firing end camera taken on 2018-05-06. Note the significant decrease in shell temperature observed in measurement areas E, F, and G.

image on the left side of Figure 10 is taken from 2018-04-29 while the image on the right side of Figure 10 is taken from 2018-05-06. Note that the right-side image exhibits significantly darker shell colors in measurement areas E, F, and G. These darker shell colors directly correspond to the shell temperature decrease observed in Figure 9. Figure 11 investigates the longer, mid-kiln temperature drop by comparing raw images taken from the thermal camera that monitors the middle section of the kiln. The image on the left side of Figure 11 is taken from 2018-05-23 whereas the image on the right side is taken from 2018-05-30. During this week of operation, measurement areas C, D, E, and H become significantly darker which corresponds to the drop in temperature observed in Figure 9 both in terms of location and time period. Further investigation can be conducted to determine whether the observed temperature decrease is due to ring formation or confounding factors related to operating variables and ambient conditions. Nevertheless, without the ability to intuitively visualize and conveniently navigate through large amounts of historical KST data, operators and engineers are burdened with flipping through large quantities of raw video or image data.



**Figure 11:** Using raw images from the mid-zone thermal camera to confirm presumed ring formation in the 23-40 m range between 2018-05-18 and 2018-06-05. Left: kiln mid-zone image taken on 2018-05-23. Right: kiln mid-zone image from 2018-05-30 exhibiting significantly colder shell temperatures. Note, measurement area A is hot in both images, but the rest of the kiln mid-zone is significantly colder in the right figure. This sudden temperature drop that is consistent across such a large area is not necessarily indicative of ring formation. Further investigation is required.

The start date and window size are conveniently selected with interactive sliders which ultimately determine the  $x$ -axis ticks. In our work we are studying the formation of rings in a rotary kiln and we have found the proposed visualization tool to be highly useful for intuitively visualizing the thermal camera data. To supplement the spatiotemporal heatmap another interactive feature is included that allows users to select from a list of process variables (PVs) to plot one below the heatmap with the same start date and window size. Axes, units, and PV descriptions are updated automatically. This feature is demonstrated in Figure 12 to further investigate the long and consistent decrease in shell temperatures found in Figure 11.



**Figure 12:** Further investigation is conducted by reducing the window size and plotting relevant operating variables alongside the heatmap visualization. **Top:** the spatiotemporal heatmap of KST profiles. **Bottom:** a sustained drop in mud solids content between 2018-05-28 and 2018-05-31 suggests the observations from the right side of Figure 11 are due to poor performance of the mud filters resulting in lime mud that is too wet. Mill records confirm mud filter problems during this period.

In this case study, further decreasing the window size and plotting suspected variables alongside the

heatmap provides an effective method of ruling out potential causes and gaining new insights. The lower plot in Figure 12 suggests the reason for the KST decrease observed in Figure 11 is poor performance of the lime mud filters resulting in too much water entering the kiln. This is shown by the sustained reduction in the mud solids percentage between 2018-05-28 and 2018-05-31. Mud filter performance is well-known as a critical factor for ensuring proper functionality and efficiency of lime kilns (Nesselrodt et al., 2015). Mill records confirm that mud filter performance was a concern during this period. Moreover, mill personnel have observed a seasonal pattern where spring runoff results in an increase in mill water turbidity and perhaps a reduction in mud filter performance. Although this drop in shell temperature may initially be due to mud moisture it is clear from Figure 8 that, at approximately 38 m from the firing end, the shell temperature does not recover until there is a mill shutdown. Ultimately, a ring does form in this area, and it needs to be manually removed during a shutdown.

## 5 Implementation

The implementation discussed in this section describes both how the visualization tool can be constructed as well as how it can be used to improve the monitoring and operation of rotary kilns. A coding tutorial in the form of an iPython notebook is provided to assist interested readers with the implementation and utilization of the proposed visualization strategy (Rippon, 2020). This tutorial uses an entirely synthetic set of data to represent different KST measurements along the length of the kiln and auxiliary PVs for additional context. The tutorial loads this synthetic data and uses Python code to generate the interactive spatiotemporal heatmap. Ultimately, the synthetic set of data can be replaced by a set of real operating data and the code provided in the tutorial can be used as a guide for creating a valuable process monitoring tool. Practitioners can extract a spreadsheet of operating data from a process historian, format it according to the synthetic data, load it into a Python environment, and run the provided code to visualize their own data. Instructions are included in the tutorial repository to help users run the iPython notebook with either a third-party web application (e.g., Google Colaboratory) or by setting up a Python environment on their local machine.

For industrial implementation, the visualization code could run on a computer that is setup to periodically update the historical set of data with recent operating data. Even without live updates the convenient and intuitive nature of this visual tool enables navigation and comprehension of large quantities of high dimensional historical data. In addition to identifying periods of fouling the spatiotemporal heatmap can be used to quickly evaluate the quality of the raw data and the effect of data pre-processing activities. Individual shutdowns can be identified, and start-up procedures can be compared. The state of the process can be succinctly compared across years of operation. Alarms can be tracked and investigated. Finally, the tools used are open-source and with some effort they can be customized to fit many applications.

## 6 Conclusions

Rotary kilns are immense, energy-intensive unit operations that play important roles in the production of pulp, cement, and other materials. Increasingly, rotary kilns are outfitted with thermal cameras that measure the temperature of the kiln shell profile over time. In this work we propose a novel strategy to intuitively visualize large quantities of shell temperature profile data over varying time scales. The visualization strategy is demonstrated with an industrial case study and shown to be effective at yielding operating insights (e.g., identifying multiscale ring formation) from the thermal camera data. Our analysis of ring formation in a rotary lime kiln has led to the development of this visualization technique which we have found to be a very helpful, convenient, and intuitive approach to visualizing large quantities of historical kiln data.

Ultimately, we aim to develop a real-time instrument that estimates ring thickness and provides causal associations that can be controlled to extend operation before manual ring removal is required. However, the contributions outlined in this paper are the result of developing enhanced tools and methods for investigating historical kiln data to gain insights and improve our development of the detection and diagnosis system. Nonetheless, the proposed visualization strategy has already improved our understanding of ring formation (e.g., problematic areas, timescales of ring formation, measurement disturbances, etc.) to the extent that we are expanding our strategy to multiple mills to better visualize their historical data. Finally, we are currently investigating options for operational application of this visualization to

assist engineers and operators and help mitigate the effects of ring formation. For those interested in implementing this visualization technique with their own kiln data we have made the code freely available at <https://github.com/LeeRippon/KilnVisual> along with a brief instructive tutorial using synthetic data (Rippon, 2020).

## References

- Danila, A. and Tamas, F. (2020). The thermal field analysis of the rotary kiln for the cement plants by means of the image processing techniques. In *IOP Conference Series: Materials Science and Engineering*, volume 789, page 012016. IOP Publishing.
- Dernegård, H., Breid, H., and Theliander, H. (2017). Characterization of a dusting lime kiln—a mill study. *Nordic Pulp and Paper Research Journal*, 32(1):25–34.
- Gorog, J. P. and Leary, W. (2016). Ring removal in rotary kilns used by the pulp and paper industry. *Tappi Journal*, 15(3):205–213.
- Gürtürk, M. and Oztop, H. F. (2014). Energy and exergy analysis of a rotary kiln used for plaster production. *Applied thermal engineering*, 67(1-2):554–565.
- Hirtz, B., Marshman, D., and Sheehan, C. (2017). Kiln infra-red cameras for abnormal situation detection and residual carbonate control. *J-for-Journal of Science & Technology for Forest Products and Processes*, 6(3):28–36.
- Keim, E., Zuniga, J., and Tran, H. (2020). Combatting lime kiln ringing problems at the arauco constitution mill. *TAPPI JOURNAL*, 19(7):345–354.
- Le Guen, L. and Huchet, F. (2020). Thermal imaging as a tool for process modelling: application to a flight rotary kiln. *Quantitative InfraRed Thermography Journal*, 17(2):79–95.
- Nesselrodt, K., Lee, S., Andrews, J. D., and Hart, P. W. (2015). Mill study on improving lime kiln efficiency. *TAPPI JOURNAL*, 14(2):133–139.
- Rippon, L. (2020). Lime kiln visualization tutorial. <https://github.com/LeeRippon/KilnVisual>.
- Smook, G. A., Kocurek, M. J., et al. (1982). *Handbook for pulp & paper technologists*. Canadian Pulp and Paper Association.
- Tran, H. (2007). Lime kiln chemistry and effects on kiln operations. *Pulp & Paper Centre and Department of Chemical Engineering and Applied Chemistry, University of Toronto, Toronto, Canada*.
- Yi, Z., Xiao, H., and Song, J. (2013). An alumina rotary kiln monitoring system based on infrared ray scanning. *Measurement*, 46(7):2051–2055.